ADVANCED FUNCTIONAL MATERIALS
www.afm-journal.de

Effect of the Threshold Kinetics on the Filament Relaxation Behavior of Ag-Based Diffusive Memristors

Solomon Amsalu Chekol, Stephan Menzel, Rana Walied Ahmad, Rainer Waser, and Susanne Hoffmann-Eifert**

Owing to their unique features such as thresholding and self-relaxation behavior diffusive memristors built from volatile electrochemical metallization (v-ECM) devices are drawing attention in emerging memories and neuromorphic computing areas such as temporal coding. Unlike the switching kinetics of non-volatile ECM cells, the thresholding and relaxation dynamics of diffusive memristors are still under investigation. Comprehension of the kinetics and identification of the underlying physical processes during switching and relaxation are of utmost importance to optimize and modulate the performance of threshold devices. In this study, the switching dynamics of Ag/HfO_2/Pt v-ECM devices are investigated. Depending on the amplitude and duration of applied voltage pulses, the threshold kinetics and the filament relaxation are analyzed in a comprehensive approach. This enables the identification of different mechanisms as the rate-limiting steps for filament formation and, consequently, to simulate the threshold kinetics using a physical model modified from non-volatile ECM. New insights gained from the combined threshold and relaxation kinetics study outline the significance of the filament formation and growth process on its relaxation time. This knowledge can be directly transferred into the optimization of the operation conditions of diffusive memristors in neuromorphic circuits.

1. Introduction

Next-generation technologies like machine learning, artificial intelligence (AI), cloud computing, and big data demand an exponential growth of the volume and complexity of data and transfer. Limited in scalability, computation power, and data transfer rates between memory and central processing unit, traditional computing architectures are suffering to persevere with the rapidly expanding demand of data storage and processing. Neuromorphic computing concepts that mimic the function of the biological brain are intensively studied as energy-efficient architectures which might overcome the von Neumann bottleneck.[1–3] Memristive devices (short: memristor for memory resistor) that change their resistance state in response to an electrical stimulus are promising candidates for use in neuromorphic circuits thanks to their scalability,[4–6] 3D stacking capability,[7–9] and low power consumption.[10–12] One interesting class of memristive devices are electrochemical metallization memories (ECMs), which are based on the formation and rupture of a conductive filament due to the movement of active metal ions such as Ag^+ and $Cu^{+(2+)}$ inside an electrolyte matrix.[13–16] Recently, the commercial memory variant of non-volatile ECM devices became popular under the product name Conductive Bridging Random Access Memory (CBRAM).[17–19]

CBRAMs cover a wide assortment of materials involving pure (ion) electrolytes such as AgI,[20] mixed ion-electron conductors (MIEC) such as Ge_xSe_{1-x},[21,22] and insulators such as SiO_2,[23,24] Ta_2O_5,[25] and HfO_2[26] typically combined with Cu, Ag, or a Cu/Ag-containing material. Recently, a subquantum CBRAM cell based on a Te alloy top electrode and an oxide electrolyte has been demonstrated for storage[27] and neuromorphic[28] applications.

Inspired by the non-volatile electrochemical memories, volatile ECMs (v-ECMs) have recently gained attention for a wide range of applications due to their unique thresholding behavior.[29–33] V-ECM devices are promising selectors for memristive crossbar arrays[34,35] as well as interesting elements for artificial neurons in neuromorphic computing,[30–31,36] and true random number generators (TRGN)[37] in network security. The working principle of v-ECM is quite similar to that of the non-volatile ECMs.[34] Initially, the device is in a high resistance state (HRS) and with the application of a positive bias to the active electrode (such as Ag or Cu), a metallic conductive filament can be formed inside the electrolyte through electron transfer and ion motion of the active material, bridging the

S. A. Chekol, S. Menzel, R. W. Ahmad, R. Waser, S. Hoffmann-Eifert
Forschungszentrum Jülich GmbH
Peter Grünberg Institute (PGI 7 and 10) and JARA-FIT
Wilhelm-Johnen-Straße, 52428 Jülich, Germany
E-mail: s.chekol@fz-juelich.de; su.hoffmann@fz-juelich.de
S. A. Chekol, R. W. Ahmad
RWTH Aachen University
Templergraben 55, 52062 Aachen, Germany
R. Waser
Institute of Materials in Electrical Engineering and Information Technology II
RWTH Aachen University
Sommerfeldstraße 24, 52074 Aachen, Germany
The ORCID identification number(s) for the author(s) of this article can be found under https://doi.org/10.1002/adfm.202111242.

DOI: 10.1002/adfm.202111242

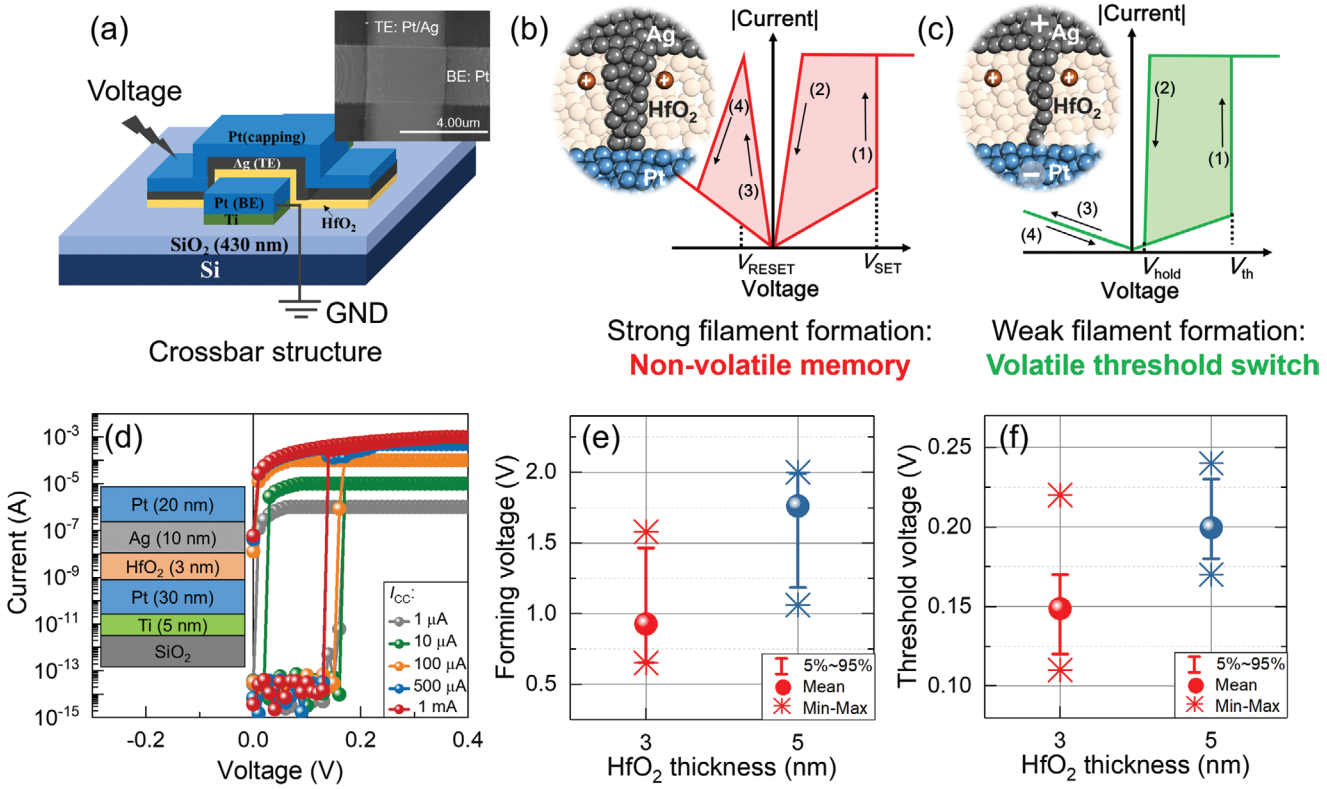

Figure 1. a) Schematic of the crossbar structure of an Ag/HfO_2/Pt device. The inset shows the top view photograph by scanning electron microscopy. The two possible switching modes of electrochemical metallization memory (ECM): The formation of a strong and weak conductive filament leads to a b) non-volatile memory and c) volatile threshold switch. d) Typical *I–V* characteristics of the Ag/HfO_2/Pt device under different values of compliance current (I_{CC}). The inset presents the full device stack and respective thicknesses. e) Forming voltage and f) threshold voltage for devices with a 3 nm and 5 nm thin HfO_2 electrolyte layer. The forming voltage is collected from 20 devices and the threshold voltage is obtained from 100 repeated cycles.

two electrodes electrically. As a result of the SET process, the resistance abruptly jumps to a much lower resistive state (LRS). The stability of this conductive filament depends on the initial filament morphology, the surrounding electrolyte matrix, and other external factors such as bias and temperature.[38] A bulky metal filament is stable and leads to non-volatile memory, which requires SET and RESET processes at opposite voltage polarity, $V_{SET,}$ and V_{RESET}, respectively (**Figure 1**b). On the contrary, a thinner or weak filament, which was closed at the threshold voltage (V_{th}) can spontaneously self-rupture and the device resistance relaxes back to the HRS if the applied voltage falls below the hold voltage (V_{hold}) yielding a volatile switch (Figure 1c). Driving forces of this self-relaxation process discussed in the literature comprise surface energy minimization or surface tension effects,[38–40] thermo-diffusion,[41] mechanical stress,[42] or steric repulsion effect[43] depending on the nature of the filament and the surrounding electrolyte matrix.

Triggered by the interest in these devices for artificial neurons, the time constants of the threshold and relaxation processes become highly relevant. In v-ECM devices, both response times can be modulated over several orders of magnitude depending on the programming condition.[34,44] This can provide a distinctive advantage of designing a system with a specific combination of SET (t_{set}) and relaxation time (t_r). However, in contrast to the solid knowledge of the fundamental processes involved in non-volatile ECM devices[45–49] the understanding of the volatile characteristic in v-ECM cells which arises via the self-rupture of the conducting filament without any external force, is still at the beginning. Wang et al. explained the relaxation process of v-ECMs based on a thermodynamic approach utilizing the surface diffusion mechanism.[38] Taking a defined filament shape and size as input parameters, good agreement of simulated and experimental data was obtained. In the experiments, the filament's strength was modified qualitatively by varying the programming current through a transistor.[50,51] On the other hand, the dependence of t_{set} on the external bias has been shown in multiple publications and, yet, lack to make connections with the t_r.[52–54] For a wide utilization of v-ECM devices in the emerging field of neuromorphic computation[55–58] understanding and control of the switching kinetics is of utmost importance. Therefore, the complete information about the influence of the programming conditions on threshold and relaxation behavior and any type of correlation is important. This is the focus of the presented study.

In this paper, a systematic investigation of the kinetics of both threshold and relaxation processes of Ag/HfO_2/Pt v-ECM devices is reported. Programming schemes with different voltage amplitude (V_p) and pulse width (t_p) were designed to explore the impact of the programming condition on the response times t_{set} and t_r. The threshold kinetics is analyzed under consideration of the rate-limiting processes using a physical simulation utilizing an extension of the dynamic

compact model, which has been successfully applied to explain the dynamics of AgI-based,[59] SiO_2-based,[49] and GeS-based[60] ECM cells (called JART ECM v1[61]). The relaxation dynamic is evaluated in the same parameter regime and is analyzed together with the threshold event. This allowed us to discuss the effect of filament morphology and diameter on the resulting t_r for the studied system.

2. Results and Discussion

2.1. Device Characteristics

In this study, micro-crossbar-type devices (Figure 1a) of 2×2 $(\mu m)^2$ in size were utilized. An Ag top electrode capped with a Pt layer served as the active metal for ion supply into the 3 and 5 nm thick HfO_2 layer. To support the electrochemical oxidation reaction through the injection of electrons, inert Pt is used as a counter/bottom electrode. The device stack and typical *I–V* sweep characteristics of the fabricated v-ECM cells are shown in Figure 1d. An abrupt and volatile switching with a wide range of compliance currents (I_{CC}) up to 1 mA is obtained. All devices are highly insulating in the pristine state and for Ag filament creation a forming process with a relatively higher voltage (V_F) than the threshold voltage (V_{th}) is required. V_F and V_{th} of the Ag/HfO_2/Pt devices with HfO_2 thicknesses of 3 and 5 nm are shown in Figure 1e and 1f, respectively. Both voltages increase with the oxide layer thickness. This trend reflects the strong field dependence of the switching behavior like it has been discussed in previous reports.[62–64] The extremely low leakage current, large on/off ratio together with a low V_{th} make these types of devices an ideal candidate for selectors in crossbar arrays and low power applications such as artificial neurons.

Furthermore, an endurance of exceeding 10^6 under switching cycles and fast switching speed are among the important factors. The temporal response of the device can be extracted from the current response in the time domain upon a voltage pulse with amplitude V_p and pulse time t_p. After a certain time period t_{set} (often called delay) referenced to the onset of the voltage pulse, the device current abruptly jumps from low to high. Once the voltage is removed, the device relaxes spontaneously back to the HRS after a definite time period of t_r (sometimes referred to as retention time) (**Figure 2**a). A typical temporal response of an Ag/HfO_2/Pt device is presented in Figure 2c. The measurement setup used to collect the temporal responses is depicted in Figure 2b (left). We used a Keithley 4200 SCS Semiconductor Characterization System equipped with four 4225 PMUs and an integrated oscilloscope card with a bandwidth of 1 GHz. An external resistor of 100 kΩ was connected in series with the device to limit the current during switching. The input voltage pulse signal is connected to the Pt/Ag top electrode while the Pt counter electrode is grounded. The corresponding input voltage and output current signals are recorded through channel 1 and channel 2 of the oscilloscope. With the application of a voltage pulse with V_p of 1.4 V and t_p of 1 µs, characteristic response times of t_{set} and t_r of <300 and <250 ns are obtained, respectively. The analysis of the SET and relaxation times concerning external

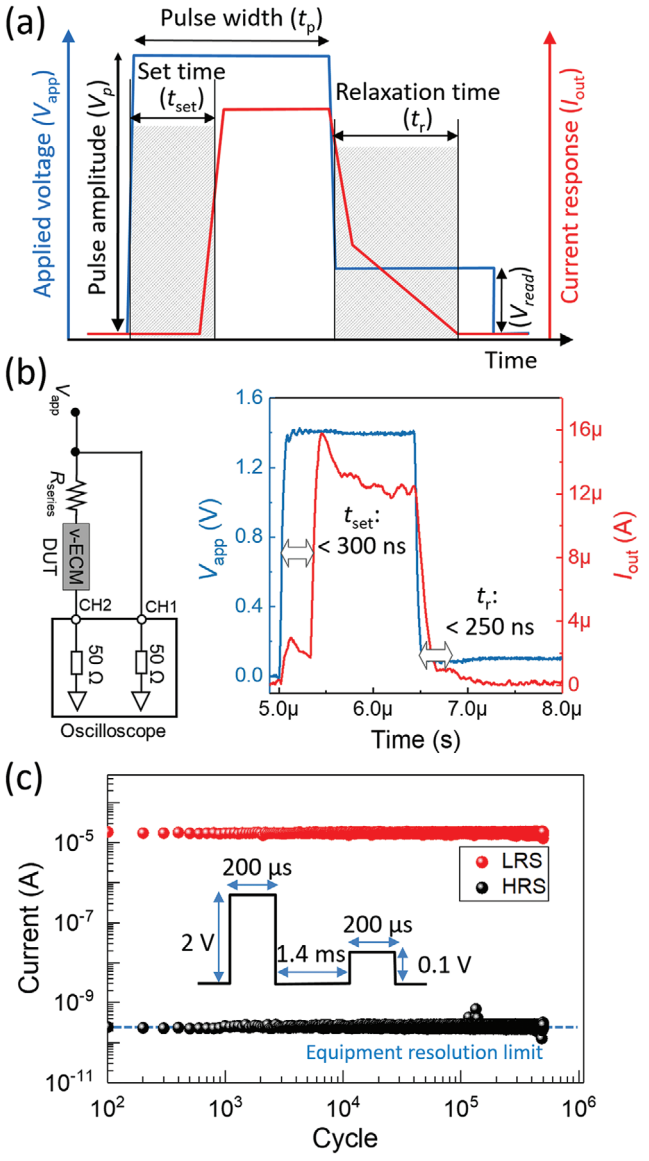

Figure 2. a) Definitions of t_{set}, and t_r from a temporal response measurement in the time domain. Blue color: applied voltage (V_{app}); red color: output current signal (I_{out}). b) Current response measurement for testing the switching speed of the device with a 1.4 V/ 1.5 µs programming pulse followed by a 0.1 V read voltage (V_{read}). The device can be switched to LRS within 300 ns and spontaneously relaxes back to HRS within 250 ns. The measurement setup is shown on the left. c) Pulse endurance measurement taken for over 5×10^5 cycles. The LRS and HRS states of the device were readout at 2 and 0.1 V, respectively, as shown in the inset. A 100 kΩ external resistor was connected in series with the device to limit the current during all measurements.

factors such as V_p and t_p will be discussed in detail in the subsequent sections.

The endurance measurement acquired using a 200 µs/2 V program and read pulse for the LRS and a 200 µs/0.1 V pulse to read the HRS is presented in Figure 2c. A series resistor of 100 kΩ was used to limit the current in LRS during the measurement. The device revealed a stable switching with more than 5×10^5 cycles without any noticeable degradation.

A waiting time of 1.4 ms between each programing and read pulses was given to allow the device to fully recover and avoid any memory effect due to unsuccessful switching events. It should be noted that this is not the endurance limit of the device, as the measurement was interrupted due to elongated measurement time.

2.2. Impact of Programming Scheme on the Relaxation of Diffusive Memristors

The time required for the filament rupture process can vary by several orders of magnitude depending on the size and morphology of the conductive filament. This means, ultimately, the relaxation process depends on the programming conditions, as this determines the filament size. The higher the V_p is, the larger is the size of the conductive filament, leading to a prolonged relaxation process. In addition to V_p, the t_p can also greatly affect the t_r.

To probe the effect of the programming condition on the relaxation process, programming pulses with varied V_p and t_p were applied in a setup shown in the inset of Figure 2b and the respective t_r were extracted (details in Figure S1b, Supporting Information). We performed ten repeated cycles for each V_p and t_p combination and data with successful SET-events were further analyzed. The results are presented in **Figure 3**. Here, t_r is defined as the time between the points in time where the voltage drops to the monitor voltage (in this case 0.1 V) and where the output current fully relaxes back to the initial state (Figure 3b). From the various programming conditions applied to the device in a defined HRS an exponential relationship between t_r and V_p is observed. When V_p increases stepwise from 0.6 V to 1.7 V, t_r increased by roughly two orders of magnitude, under a fixed t_p varied between 10 µs and 10 ms, (Figure 3c). Notably, an increase in t_p shifts the linear $\log(t_r) - V_p$ dependencies upwards in time without any pronounced change in the slope. Figure 3d shows the observed power-law relation between t_r and t_p.

The relaxation process is, in a sense, a trace of the device's history. The t_r tells us how weak or strong the formed filament was. Therefore, to fully understand the relaxation behavior, it is important to look into the SET kinetics, where the filament formation happens, in detail.

2.3. Impact of Voltage on the SET Kinetics of Diffusive Memristors

Switching speed is a very crucial parameter for device operation. The exponential dependence of t_{set} with V_p for v-ECMs has been shown in multiple publications.[54,65] Many of these reports solely assume nucleation energy as a limiting factor for the switching speed. However, it has been shown that the filament growth dynamics can be significantly limited by the ion migration process and this in fact can affect the switching kinetics.[66,67] Furthermore, in-depth investigation on the SET kinetics of v-ECM devices based on reasonably large statistical

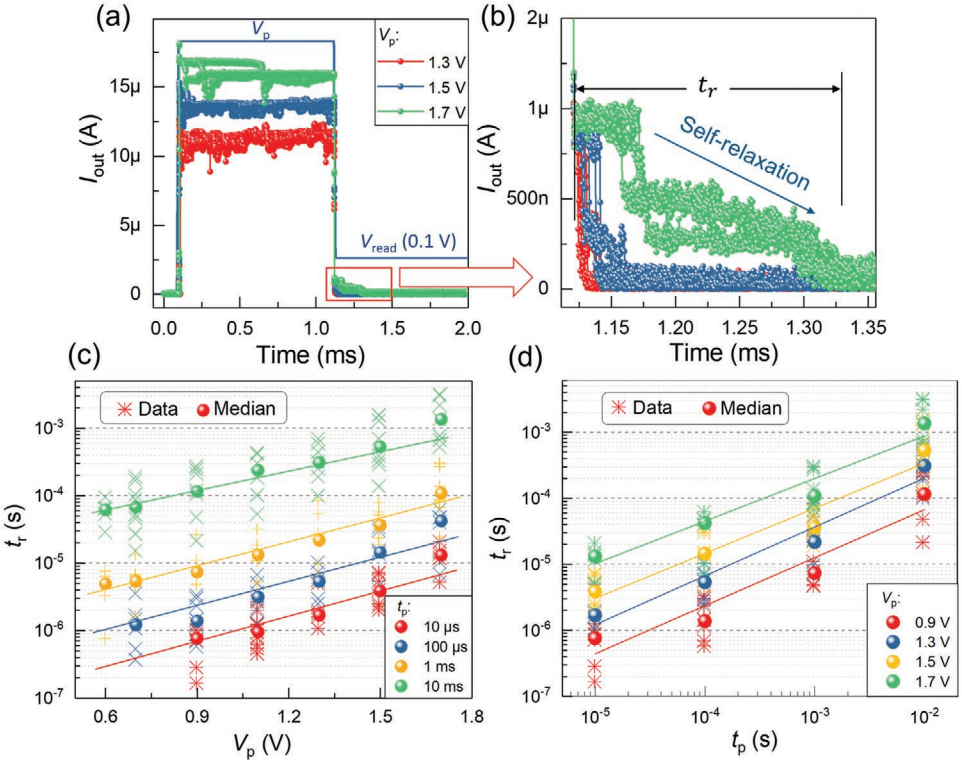

Figure 3. a) Typical current response, I_{out}-t, under programming pulses V_p/ t_p of 1.3 V, 1.5 V, and 1.7 V/ 1 ms followed by a 0.1 V voltage step for monitoring the relaxation behavior. b) Magnified plot of the red marked region in (a). The self-relaxation process takes different times t_r depending on the various programming conditions. The statistical analysis of ten repetitions for each V_p/ t_p combination provides information on t_r as a function of V_p and t_p shown in (c) and (d), respectively. The measurement setup is shown in Figure 2b.

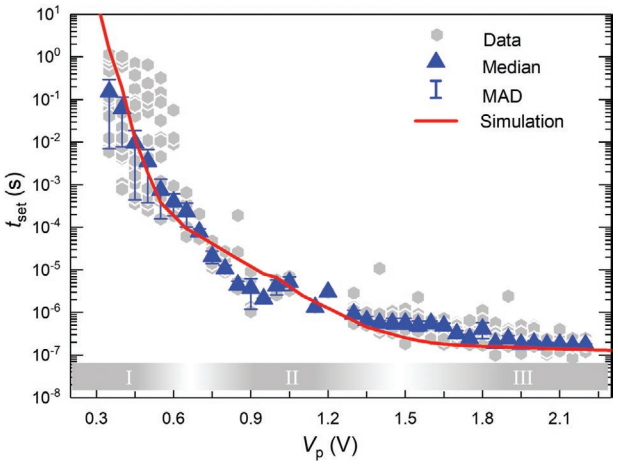

Figure 4. SET switching kinetics of Ag/HfO_2/Pt v-ECM cells with an HfO_2 thickness of 3 nm and a device size of 2 µm × 2 µm. The median values and median absolute deviation (MAD) of the experimental data are displayed using triangles and vertical lines, respectively. The three regions, I, II, and III represent the nucleation-limited, the electron-transfer-limited, and the mixed control regimes, respectively. The fitting data acquired from the numerical simulation is shown as red solid line. The circuit schematics used for testing with a load resistor of 100 kΩ is shown in Figure 2b.

data sets has not been shown so far. Thus, to better understand and pinpoint the physical processes involved not only during nucleation but also during filament growth we conducted a thorough analysis of the switching kinetics of volatile switching Ag/HfO_2/Pt devices by designing different programming schemes.

Devices in HRS were excited by defined voltage pulses with varying V_p ranging from 0.35 to 2.2 V and t_p of 1 µs to 1 s and the corresponding value of the switching time t_{set} was extracted from the transient current response (details in Figure S1a, Supporting Information). A typical series of I_{out}–t curves for different V_p is shown in Figure S2, Supporting Information. **Figure 4** presents the experimental results of t_{set} as a function of V_p. At a low voltage regime, the switching takes a longer time to be triggered and a slight increase in V_p dramatically reduces t_{set}. With a further increase of V_p, the corresponding decrease in t_{set} continuously flattens and appears to approach a kind of saturation at higher V_p. Menzel et al. have reported similar observations for AgI-based non-volatile ECMs. These authors identified three regimes by means of the rate-determining step as (I) nucleation limited, (II) electron transfer limited, and (III) mixed (electron-transfer and ion migration) limited.[59]

Therefore, to further investigate the physical processes limiting the switching speed of our Ag/HfO_2/Pt-based v-ECMs, we implemented the well-verified simulation model developed by one of the authors.[59] In general, the formation of conductive filament proceeds in two steps: nucleation and growth. Nucleation is a very critical process for further growth of the filament, and, depending on the voltage it can take a significantly long time. The nucleation time can be described by the following equation:[59]

$$t_{nuc} = t_{0,nuc} \exp\left(\frac{\Delta G_{nuc}}{k_B T}\right)\exp\left(-\frac{(N_C + \alpha_{nuc})ze}{k_B T}\Delta\varphi_{nuc}\right) \quad (1)$$

Here, $t_{0,nuc}$ is a prefactor, ΔG_{nuc} defines the activation energy for nucleation, $\Delta\varphi_{nuc}$ the nucleation overpotential, N_C the number of Ag atoms required to form the critical nucleus, z the ion charge number, e the electron charge, α_{nuc} the charge transfer coefficient during nucleation, k_B the Boltzmann constant, and T the absolute temperature in Kelvin.

During the filament growth process, two components contribute to the current passing through the device; the ionic current and the electronic current. The electronic current is given by electron tunneling (Equation (2)) between the growing filament and the opposing electrode. The ionic current paths consist of the electron–transfer (Butler–Volmer-law, Equation (3)) and the metal/oxide interfaces, and the ion hopping (Mott–Gurney-law, Equation (4)), and their respective values can be calculated as the following.[59]

$$I_{tu} = C\frac{3\sqrt{2m_{eff}\Delta W_0}}{2x}\left(\frac{e}{h}\right)^2 \exp\left(-\frac{4\pi x}{h}\sqrt{2m_{eff}\Delta W_0}\right)A_{fil}V_{tu} \quad (2)$$

$$I_{fil/ac} = \pm zeck_{0,et}\exp\left(-\frac{\Delta G_{et}}{k_B T}\right)\left[\exp\left(\frac{(1-\alpha_{et})ze}{k_B T}\Delta\varphi_{fil/ac}\right) - \exp\left(-\frac{\alpha_{et}ze}{k_B T}\Delta\varphi_{fil/ac}\right)\right]A_{fil/ac} \quad (3)$$

$$I_{hop} = 2zecaf\exp\left(-\frac{\Delta G_{hop}}{k_B T}\right)\sinh\left(\frac{aze\Delta\varphi_{hop}}{2k_B Tx}\right)A_{is} \quad (4)$$

m_{eff} denotes the effective electron mass, ΔW_0 the tunneling barrier height, h Planck's constant, A_{fil} the area of the filament, A_{is} equivalent area of ionic conduction, V_{tu} the voltage over the tunneling barrier, c is the Ag^+ ion concentration, ΔG_{et} and ΔG_{hop} are the activation energies for electron-transfer and hopping barrier, respectively, α_{et} is the charge transfer coefficient, a is the hopping distance, $\Delta\phi_{fil/ac}$ is the electron-transfer overpotential, and $\Delta\phi_{hop}$ is the hopping over potential. C is a fitting parameter with a given value of 2.7.[59] The state variable x describes the tunneling gap between the growing filament and the electrode.

In Figure 4, the simulation results are shown as a solid line together with the experimental data. The parameters used to fit the data are presented in **Table 1**. From the measurement, three distinct regimes can be observed. The highest slope can be seen at voltages below 0.6 V in regime I which is classified as the nucleation-limited regime. Then, subsequently, a flatter slope is observed in voltage range II between 0.6 and 1.5 V where the electron-transfer reaction is the rate-limiting process. Above 1.5 V regime III with a mixed electron-transfer and silver ion hopping limited process is visible with minor voltage dependence on t_{set}.

2.4. Interdependence of SET and Relaxation Processes

At this point, there exists an obvious trade-off between t_{set} and t_r with respect to the programming conditions. The dependence on the voltage of the SET pulse V_p is schematically depicted in **Figure 5**a. For example, a shorter t_{set} can be achieved by increasing V_p, however, at the price of a prolonged relaxation process described by means of t_r. Because t_{set} defines the delay

Table 1. Parameters used to fit the SET kinetics in Figure 4.

Symbol	Value	Symbol	Value
T	298 K	ΔG_{et}	0.62 eV
z	1	α_{et}	0.3
m_r	0.84	$k_{0,et}$	2×10^3 m s^{-1}
f	1×10^{13} Hz	ΔG_{hop}	0.21 eV
c	3×10^{28} m^{-3}	a	0.25 nm
ρ_{Ag}	1.7×10^{-8} Ωm	L	3 nm
ΔW_0	2.7 eV	A_{fil}	3.14 nm^2
N_c	1	A_{is}	3.14 nm^2
ΔG_{nuc}	0.84 eV	A_{AC}	314.16 nm^2
α_{nuc}	0.25	R_{el}	1.11 mΩ
$t_{0,nuc}$	2×10^{-7} s	R_{series}	100 kΩ

time between the voltage pulse starts and the abrupt rising in current, there is no correlation between t_{set} and t_p provided that $t_p \geq t_{set}$ holds for a given value of V_p. This is described by the horizontal line in Figure 5b. In contrast, a linear relationship is observed between $\log(t_r)$ and $\log(t_p)$ (see Figure 3d), which will be analyzed further in the following.

This interdependence is visualized in a heat map given in Figure 5c, which summarizes the correlation between t_{set} and t_r as a function of V_p and t_p. The experimental results of this work are provided in the color code. In addition, further t_r data collected from different reports on Ag-based v-ECM cells are overlaid on top of the heat map for comparison, and a similar trend of the t_r versus V_p and t_p behavior is observed. The SET kinetics t_{set}–V_p from Figure 4 is given as the dashed line which separates the regime of no switching (HRS) in the bottom left corner of Figure 5c from the regime of successful SET events expanding to the upper right corner. For the remaining V_p–t_p combinations which define successful SET events, the relaxation behavior of the filament given by t_r depends on both V_p and t_p. For example, by increasing the t_p from 10 µs to 10 ms (moving upward direction in Figure 5c), the t_r changes by several orders of magnitude. In our study, it is found that the minimum t_p for a successful SET event at any given V_p gives the minimum t_r.

The analysis of the interdependence of the SET and the relaxation process that is summarized in Figure 5c now enables a

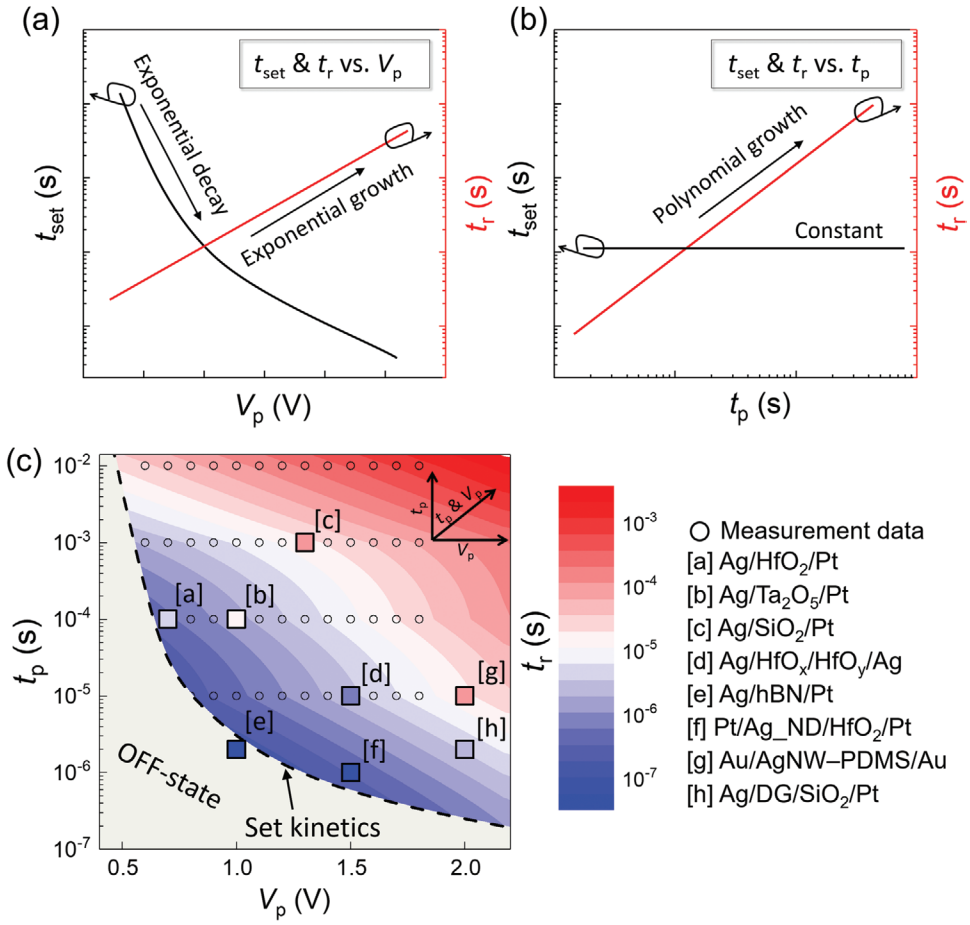

Figure 5. a,b) Schematic representation of the dependence of t_{set} and t_r as a function of V_p and t_p, respectively. c) A heat map combining the SET kinetics and relaxation event showing several orders of magnitude change in t_r over a certain range of V_p and t_p. The SET kinetics curve (dashed line) is a representative fitting curve of experimentally obtained data. The color-coded relaxation time is plotted based on experimental data (open circles) and an extrapolation. Letter assigned boxes are relaxation data collected from different publications (**Table 2**).

Table 2. Ag-based threshold switching devices used to collect the relaxation data points in Figure 5c.

Symbol	Device stack	Switching layer thickness	Threshold voltage	SET pulse condition (Voltage/Pulse width)	SET time	Relaxation time	Ref.
[a]	$Ag/HfO_2/Pt$	4.5 nm	0.30 V	0.7 V/100 µs	N/A	10 µs	[65]
[b]	$Ag/Ta_2O_5/Pt$	5 nm	0.35 V	1.0 V/100 µs	2.5 µs	15 µs	[68]
[c]	$Ag/SiO_2/Pt$	30 nm	0.70 V	1.3 V/1 ms	N/A	100 µs	[69]
[d]	$Ag/HfO_x/HfO_y/Ag$	30 nm	0.28 V	1.5 V/10 µs	634 ns	10 µs	[70]
[e]	Ag/hBN/Pt	0.33 nm	0.30 V	1.0 V/2 µs	150 ns	60 ns	[71]
[f]	$Pt/Ag\_ND/HfO_2/Pt$	8 nm	0.50 V	1.5 V/1 µs	75 ns	300 ns	[54]
[g]	Au/AgNW–PDMS/Au	N/A	0.40 V	2.0 V/10 µs	520 ns	110 µs	[32]
[h]	$Ag/DG/SiO_2/Pt$	40 nm	0.50–1.00 V	2.0 V/2 µs	100 ns	1 µs	[72]

Note: N/A, not available.

deeper understanding of the linear dependencies of the $\log(t_r)$–V_p and $\log(t_r)$–$\log(t_p)$ behavior reported in Figures 3c and 3d, respectively. Similar trends observed earlier are described in references[34,44,54] for example. Experimentally obtained results show that for a voltage pulse of a given amplitude V_p the pulse time t_p in fact can change t_r by several orders of magnitude and, so far, this has been simply interpreted as a change in the strength of the metallic filament. However, by the combination of the threshold and relaxation behavior, we are now able to conclude that a more detailed description of the filament's growth process is required to understand the complex correlation displayed in Figure 5c.

2.5. Origin of the Relaxation Time Dependence on Programming Pulse Width

From the correlation plot in Figure 5c, an important question arises: How can a fixed pulse voltage V_p which corresponds to a defined SET time t_{set} for closing the conductive filament lead to relaxation times t_r that vary by orders of magnitude simply by enlarging the pulse time t_p? This becomes even more challenging as t_{set}–V_p follows the well-understood growth mechanism described by the SET kinetics in Section 2.3. To further explore this, we carefully analyzed the transient signals during switching together with the experimental setup that was used to obtain the data. The origin was found in the voltage divider built by the chosen R_{series} of 100 kΩ and the device in LRS (see Figure 2b). Therefore, we extracted the device resistance (R_m) in LRS and calculated the respective voltage drop on the device (V_m) for a given V_p. This procedure was enabled thanks to full access to the transient signals recorded during the measurements. Further details on the calculation can be found in the supplementary material. It can be seen that R_m slowly decreases with time under constant V_p (Figure S3a, supplementary information). The calculated V_m reveals that a residual voltage drop of about 0.15–0.20 V existed throughout the pulse duration depending on R_m (Figure S3b, Supporting Information). From this analysis, we can conclude that, once the v-ECM device is switched into the LRS, a small residual voltage drop of a fraction of the pulse voltage is sufficient to keep the filament growing during the SET event.

2.6. Filament Evolution during SET Process and Relaxation Behavior

Triggered by the interest in neuromorphic applications the self-relaxation behavior in diffusive memristors became a hot research topic. Most reasonable models tend to attribute the self-diffusion process to surface energy minimization or surface tension as this accounts for the recent transmission electron microscopy (TEM) observations of the presence of clusters composed of the active Ag or Cu element. Wang et al. reported the spontaneous formation of nanoclusters during relaxation in a planar Au/SiO_xN_y:Ag/Au device by using in situ high-resolution (HR) TEM.[30] Similar observations were reported by employing an atom probe equipped HRTEM and scanning electron microscopy (SEM).[62,72–74] Additionally, recent molecular dynamic simulations confirmed the spontaneous breakdown of a continuous nanoscale Ag filament inside an oxide matrix without any external forces.[38] According to this model, t_r should strongly depend on the filament size and follow Herring's scaling law: $t_r \propto r_o^4$, where r_o defines the filament radius. For example, Figure 3c shows a four-order of magnitude change in t_r with a combined effect of V_p and t_p. Accordingly, based on Herring's scaling law, a filament radius change by an order of magnitude would be required to achieve such a change in t_r.

Note that the on-state current is limited by the series resistor (100 kΩ) and with an applied voltage between 0.6 and 1.8 V the on-state current only increases from roughly 6 µA to about 18 µA. This current level should not contribute to significant filament growth and would hardly change the radius by an order of magnitude. Therefore, the filament size and morphology is mainly determined by the kinetically limiting process and corresponding biasing condition such as voltage and duration.

From Figure 4 it becomes apparent that the experimental data obtained in the electron-transfer region do not agree well with the simulation curve that assumes a constant filament radius independent of the voltage amplitude. Previous kinetic Monte Carlo (KMC) simulations performed by one of the authors[45] predict a structural change of the metal filament from a bulkier to a fragile appearance when the switching voltage is increased. This observation is understood by a transition from dominantly isotropic to field-driven anisotropic growth at low and high pulse amplitudes, respectively.

Therefore, we investigated the effect of filament size on the SET kinetics. Simulations with different, though still

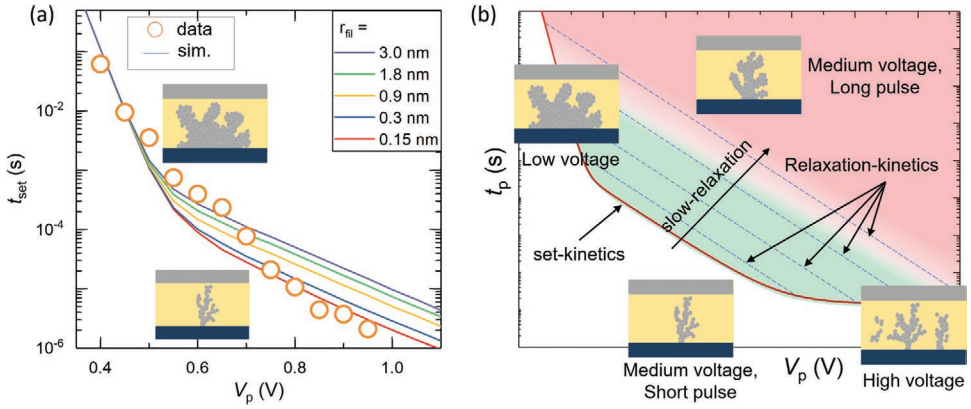

Figure 6. a) SET time as a function of pulse voltage simulated for different filament radii ranging from 0.15 to 3 nm. b) Schematic representation of the filament morphology at different combinations of V_p and t_p.

voltage-independent, filament radii ranging from 0.15 to 3.0 nm were performed using the full numerical simulation and the results are displayed in **Figure 6**a. Particularly in the electron-transfer region (II), the influence of filament radius on the t_{set} becomes significant. Suggesting that different filament radii are to be expected at different voltage regions provides a good fit to the experimentally determined SET kinetics values. In detail, for the SET event Figure 6a predicts a decrease of the filament radius from about 3.0–0.15 nm as the voltage pulse increases from roughly 0.5 V to about 1.0 V. Data points below 0.15 nm, the atomic radius of a single Ag atom, could be understood as successful SET events that do not result in a galvanic contact. Detailed investigation of the conduction mechanisms, the directionality of the switching, and filament retraction during relaxation can be found in Section S1.1, Supporting Information.

In total, the dependence of the filament radius on the pulse voltage affects the SET kinetics, especially in the electron transfer regime. Although this effect is less pronounced than the power of the four-law for the relaxation time, $t_r \propto r_0^4$, the combination of the two phenomena results in significant consequences for the programming regime of v-ECM-type diffusive memristors. The effect of biasing conditions on the filament formation and consequently on the SET and relaxation processes are explained as follows: At a lower voltage regime of below 0.6 V nucleation becomes the rate-limiting process. That means there are enough Ag^+-ions available for filament formation and, as a result, a relatively homogenous growth and a relatively bulky filament are expected (Figure 6b). The rupture of this takes a long time. Note that a longer t_{set} is required at low voltages. Hence, both the SET and relaxation processes take longer in the low voltage regime where nucleation becomes the rate-limiting step for the SET event. In the intermediate region, electron-transfer limits the filament's growth rate during SET, and the Ag^+-ion generation and reduction rates are very similar. As a result, linear growth of a dendritic-shaped filament occurs. The final size of the filament depends on the total pulse time t_p. With a short pulse, that is just enough to cause a successful SET event, a thin filament can be formed and ultimately shorter t_r can be achieved. However, if longer than necessary pulses are used the excess time after the switching contributes to further growth of the filament, thus, causing an increase of t_r. In the medium-high voltage region, ion migration becomes a limiting factor. That means the supply of Ag^+-ions is limited due to the migration barrier. As a consequence, local depletion of Ag^+-ions creates a field enhancement in this region, causing a self-acceleration of the filament growth. This results in a more anisotropic filament growth leading to a structure of thin dendrites. However, due to the self-acceleration and field-enhancement effect, the filament formation is much faster and any extra time beyond t_{set} will lead to the formation of a rather large filament, thus extending the relaxation process. Further increase in voltage will lead to extremely fast and uncontrolled filament formation, and possibly an excessive loading of Ag^+ into the matrix, due to the very high electric field. This can cause a delay in t_r by modifying the chemical potential of the matrix surrounding the filament. A schematic representation of the voltage-dependent filament growth can be found in the supplementary information, Figure S4.

2.7. Design Rule of Diffusive Demristors for Emerging Applications

The tunability of the SET and the relaxation behavior of v-ECM-type diffusive memristors with the programming conditions allow the design of systems with a particular t_{set} and t_r, depending on the desired application. For example, a fast switching time is necessary for selector devices in a cross-point array to access the memory state within a few ns. At the same time, a fast relaxation and recovery to the highly resistive state is essential to effectively block the current in the unselected memory cells during a random access operation. On the other hand, the relaxation behavior becomes more relevant in neuromorphic applications. For integrate-and-fire neurons, the device resistance should relax back to the resting state to be able to fire continuously during the application of a pulse train. If one aims to use volatile devices to store eligibility traces of the neural activity, the weight update depends on the t_r of the volatile device. This underlines the importance of the fact that the dependency of SET and relaxation processes on the programing condition provides a unique opportunity to design a system with a specific combination of t_{set} and t_r. An example of a broad variety of applications for volatile diffusive memristors which become accessible thanks to this behavior is schematically presented in **Figure 7**.

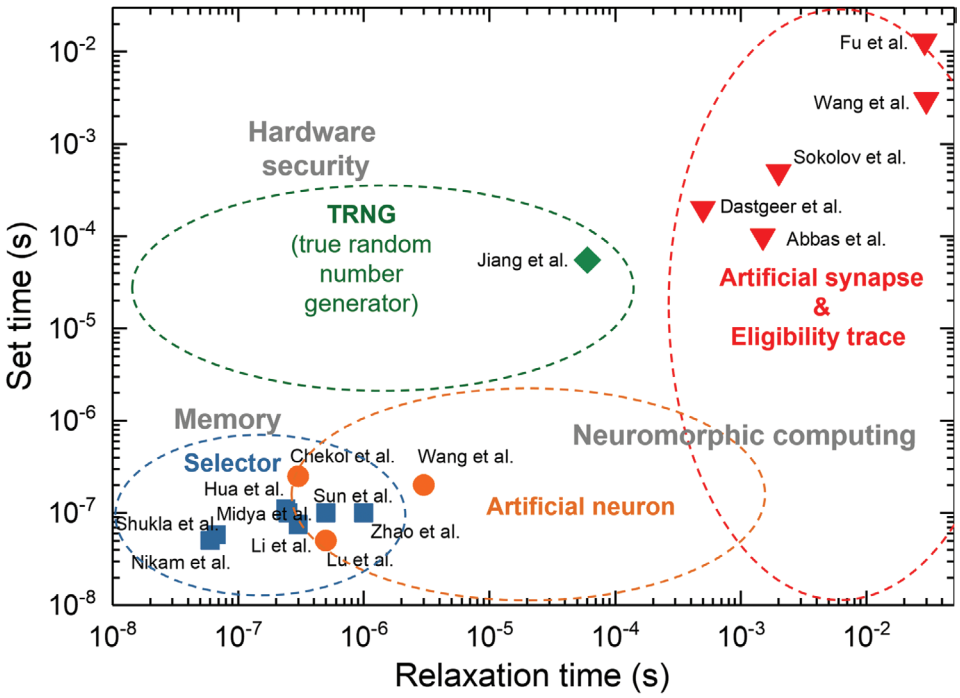

Figure 7. Different areas of applications of v-ECM-type diffusive memristors arranged according to exemplary requirements in t_{set} and t_r. Inset are t_{set} and t_r data collected from different references.[30,33,34,37,54,62,71,72,75–82]

3. Conclusion

Concluding, we investigated the switching dynamics of an Ag/HfO_2/Pt-based diffusive memristor and showed the tunability of the SET and relaxation times over several orders of magnitude depending on the programming conditions. Three main mechanisms, namely, nucleation, electron-transfer, and mixed (electron-transfer and ion-migration) are identified as the rate-limiting steps during the SET process. The relaxation time of diffusive memristors is mainly determined by the size and morphology of the conductive filament. Depending on the rate-limiting step during the SET process, different filament growth mechanisms are expected. At low voltages the growth is dominantly isotropic, resulting in a rather bulky filament and at higher voltages, the growth becomes field-driven and anisotropic yielding a thin and fragile filament. In addition to the voltage amplitude, the voltage pulse width affects the relaxation time. It is revealed that this is mainly due to the small voltage drop over the device during the on-state, contributing to further growth of the filament. These findings provide useful information for optimizing the operating conditions of diffusive memristors in neuromorphic circuits.

4. Experimental Section

Fabrication of the v-ECM Device: The micro-crossbar devices were fabricated on a SiO_2/Si substrate starting with the sputter deposition of a Ti (5 nm) adhesion layer followed by a Pt (30 nm) bottom electrode (BE), which were lithographically patterned and structured by reactive ion beam etching. The homogeneous 3 and 5 nm thin HfO_2 films with low defect concentration were grown in a plasma-enhanced atomic layer deposition (PE-ALD) process from tetraethyl-methyl-ammonia hafnium (TEMA-Hf) and oxygen plasma at 250 °C.[83,84] Following dielectric deposition, feature size ranging from 2 nm to 10 µm were patterned by photolithography. Final crossbar structures were obtained by sputter deposition of an Ag/Pt (10/20 nm) top electrode accompanied by a lift-off process.

Device Measurement and Characterization: All electrical characterizations were carried out in a probe station. The voltage sweep measurements were performed by using an Agilent B1500A semiconductor device parameter analyzer equipped with high-resolution source and measurement units. Short pulse experiments were performed by using a Keithley 4200 SCS semiconductor characterization setup equipped with 4225 PMUs and an integrated oscilloscope card with a maximum bandwidth of 1 GHz. While the input signal is applied to the Pt/Ag top electrode, the applied voltage is measured in parallel on channel 1 of the oscilloscope (internal impedance 50 Ω). The output current can be calculated from the post DUT (Pt counter electrode) signal measured on channel 2 (internal impedance 50 Ω). A custom-built tungsten probe tip with an SMD (surface mounted device) resistor of 100 kΩ was used to limit the current during switching.

Supporting Information

Supporting Information is available from the Wiley Online Library or from the author.

Acknowledgements

This work was in part funded by the German Research Foundation (DFG) under Grant No. SFB 917, in part by the Federal Ministry of Education and Research (BMBF, Germany) in the project NEUROTEC (Project Nos. 16ES1134 and 16ES1133K) and is based on the Jülich Aachen Research Alliance (JARA-FIT). The authors would like to

thank Felix Cüppers, Stephan Aussen, and Stefan Wiefels for fruitful discussions. Support of Grigory Potemkin and Clemens Wiedenhöft in sample fabrication and of Marcel Gerst for technical assistance is gratefully acknowledged.

Open access funding enabled and organized by Projekt DEAL.

Conflict of Interest

The authors declare no conflict of interest.

Data Availability Statement

The data that support the findings of this study are available from the corresponding author upon reasonable request.

Keywords

electrochemical metallization, diffusive memristor, relaxation time, switching kinetics, threshold switching, volatile switches

Received: November 5, 2021
Revised: December 6, 2021
Published online:

[1] M. A. Zidan, J. P. Strachan, W. D. Lu, *Nat. Electron.* **2018**, *1*, 22.
[2] C. S. Poon, K. Zhou, *Front. Neurosci.* **2011**, *5*, 108/1.
[3] B. Chen, F. Cai, J. Zhou, W. Ma, P. Sheridan, W. D. Lu, in *2015 IEEE Int. Electron Devices Meeting (IEDM)*, IEEE, Piscataway, NJ **2015**.
[4] D.-H. Kwon, K. M. Kim, J. H. Jang, J. M. Jeon, M. H. Lee, G. H. Kim, X.-S. Li, G.-S. Park, B. Lee, S. Han, M. Kim, C. S. Hwang, *Nat. Nanotechnol.* **2010**, *5*, 148.
[5] K. Terabe, T. Hasegawa, T. Nakayama, M. Aono, *Nature* **2005**, *433*, 47.
[6] S. Pi, C. Li, H. Jiang, W. Xia, H. Xin, J. J. Yang, Q. Xia, *Nat. Nanotechnol.* **2019**, *14*, 35.
[7] J. Y. Seok, S. J. Song, J. H. Yoon, K. J. Yoon, T. H. Park, D. E. Kwon, H. Lim, G. H. Kim, D. S. Jeong, C. S. Hwang, *Adv. Funct. Mater.* **2014**, *24*, 5316.
[8] D. B. Strukov, R. S. Williams, *Proc. Natl. Acad. Sci. USA* **2009**, *106*, 20155.
[9] P. Lin, C. Li, Z. Wang, Y. Li, H. Jiang, W. Song, M. Rao, Y. Zhuo, N. K. Upadhyay, M. Barnell, Q. Wu, J. J. Yang, Q. Xia, *Nat. Electron.* **2020**, *3*, 225.
[10] Y. LeCun, Y. Bengio, G. Hinton, *Nature* **2015**, *521*, 436.
[11] R. Waser, M. Aono, *Nat. Mater.* **2007**, *6*, 833.
[12] E. Shiu, S. Lim, in *2017 IEEE 9th Int. Memory Workshop (IMW)*, IEEE, Piscataway, NJ **2017**.
[13] R. Waser, R. Dittmann, G. Staikov, K. Szot, *Adv. Mater.* **2009**, *21*, 2632.
[14] H.-S. P. Wong, H.-Y. Lee, S. Yu, Y.-S. Chen, Y. Wu, P.-S. Chen, B. Lee, F. T. Chen, M.-J. Tsai, *Proc. IEEE* **2012**, *100*, 1951.
[15] S. Menzel, U. Böttger, M. Wimmer, M. Salinga, *Adv. Funct. Mater.* **2015**, *25*, 6306.
[16] I. Valov, W. Lu, *Nanoscale* **2016**, *8*, 13828.
[17] M. Kund, G. Beitel, C. U. Pinnow, T. Roehr, J. Schumann, R. Symanczyk, K. D. Ufert, G. Mueller, *IEDM Tech. Dig.* **2005**, 754.
[18] R. Fackenthal, M. Kitagawa, W. Otsuka, K. Prall, D. Mills, K. Tsutsui, J. Javanifard, K. Tedrow, T. Tsushima, Y. Shibahara, G. Hush, in *2014 IEEE Int. Solid-State Circuits Conf. Digest of Technical Papers (ISSCC)*, IEEE, Piscataway, NJ **2014**, p. 338.
[19] M. N. Kozicki, H. J. Barnaby, *Semicond. Sci. Tech.* **2016**, *31*, 113001.
[20] I. Valov, I. Sapezanskaia, A. Nayak, T. Tsuruoka, T. Bredow, T. Hasegawa, G. Staikov, M. Aono, R. Waser, *Nat. Mater.* **2012**, *11*, 530.
[21] C. Schindler, K. Szot, S. Karthäuser, R. Waser, *Phys. Status Solidi RRL* **2008**, *2*, 129.
[22] R. Soni, P. Meuffels, G. Staikov, R. Weng, C. Kuegeler, A. Petraru, M. Hambe, R. Waser, H. Kohlstedt, *J. Appl. Phys.* **2011**, *110*, 054509.
[23] S. Tappertzhofen, H. Mündelein, I. Valov, R. Waser, *Nanoscale* **2012**, *4*, 3040.
[24] M. Lübben, F. Cüppers, J. Mohr, M. von Witzleben, U. Breuer, R. Waser, C. Neumann, I. Valov, *Sci. Adv.* **2020**, *6*, eaaz9079.
[25] T. Tsuruoka, T. Hasegawa, I. Valov, R. Waser, M. Aono, *AIP Adv.* **2013**, *3*, 032114.
[26] M. Haemori, T. Nagata, T. Chikyow, *Appl. Phys. Express* **2009**, *2*, 061401.
[27] J. R. Jameson, D. Kamalanathan, *Appl. Phys. Lett.* **2016**, *108*, 053505.
[28] Y. Shi, L. Nguyen, S. Oh, X. Liu, F. Koushan, J. R. Jameson, D. Kuzum, *Nat. Commun.* **2018**, *9*, 5312.
[29] J. Song, J. Woo, J. Yoo, S. A. Chekol, S. Lim, C. Sung, H. Hwang, *IEEE Trans. Electron Devices* **2017**, *64*, 4763.
[30] Z. Wang, S. Joshi, S. E. Savel'ev, H. Jiang, R. Midya, P. Lin, M. Hu, N. Ge, J. P. Strachan, Z. Li, Q. Wu, M. Barne, G. Li, H. L. Xin, R. S. Williams, Q. Xia, J. J. Yang, *Nat. Mater.* **2017**, *16*, 101.
[31] Z. Wang, S. Joshi, S. Savel'ev, W. Song, R. Midya, Y. Li, M. Rao, P. Yan, S. Asapu, Y. Zhuo, H. Jiang, P. Lin, C. Li, J. H. Yoon, N. K. Upadhyay, J. Zhang, M. Hu, J. P. Strachan, M. Barnell, Q. Wu, H. Wu, R. S. Williams, Q. Xia, J. J. Yang, *Nat. Electron.* **2018**, *1*, 137.
[32] M. Wang, W. Wang, W. R. Leow, C. Wan, G. Chen, Y. Zeng, J. Yu, Y. Liu, P. Cai, H. Wang, D. Ielmini, X. Chen, *Adv. Mater.* **2018**, *30*, 1802516.
[33] S. A. Chekol, F. Cüppers, R. Waser, S. Hoffmann-Eifert, in *2021 IEEE 13th Int. Memory Workshop (IMW)*, IEEE, Dresden, Germany **2021**.
[34] R. Midya, Z. Wang, J. Zhang, S. E. Savel'ev, C. Li, M. Rao, M. H. Jang, S. Joshi, H. Jiang, P. Lin, K. Norris, N. Ge, Q. Wu, M. Barnell, Z. Li, H. L. Xin, R. S. Williams, Q. Xia, J. J. Yang, *Adv. Mater.* **2017**, *29*, 1604457.
[35] M. Rao, W. Song, F. Kiani, S. Asapu, Y.e Zhuo, R. Midya, N. Upadhyay, Q. Wu, M. Barnell, P. Lin, C. Li, Z. Wang, Q. Xia, J. J. Yang, *Small Sci.* **2021**, 2100072.
[36] Y. Zhuo, R. Midya, W. Song, Z. Wang, S. Asapu, M. Rao, P. Lin, H. Jiang, Q. Xia, R. S. Williams, J. J. Yang, *Adv. Electron. Mater.* **2021**, 2100696.
[37] H. Jiang, D. Belkin, S. E. Savel'ev, S. Lin, Z. Wang, Y. Li, S. Joshi, R. Midya, C. Li, M. Rao, M. Barnell, Q. Wu, J. J. Yang, Q. Xia, *Nat. Commun.* **2017**, *8*, 882.
[38] W. Wang, M. Wang, E. Ambrosi, A. Bricalli, M. Laudato, Z. Sun, X. Chen, D. Ielmini, *Nat. Commun.* **2019**, *10*, 9.
[39] C. P. Hsiung, H. W. Liao, J. Y. Gan, T. B. Wu, J. C. Hwang, F. Chen, M. J. Tsai, *ACS Nano* **2010**, *4*, 5414.
[40] I. Valov, E. Linn, S. Tappertzhofen, S. Schmelzer, J. v. d. Hurk, F. Lentz, R. Waser, *Nat. Commun.* **2013**, *4*, 1771.
[41] P. Bousoulas, D. Sakellaropoulos, C. Papakonstantinopoulos, S. Kitsios, C. Arvanitis, E. Bagakis, D. Tsoukalas, *Nanotechnology* **2020**, *31*, 454002.
[42] S. Ambrogio, S. Balatti, S. Choi, D. Ielmini, *Adv. Mater.* **2014**, *26*, 3885.
[43] J. Song, J. Woo, A. Prakash, D. Lee, H. Hwang, *IEEE Electron Device Lett.* **2015**, *36*, 681.
[44] Z. Wang, S. Joshi, S. E. Savel'ev, H. Jiang, R. Midya, P. Lin, M. Hu, N. Ge, J. P. Strachan, Z. Li, Q. Wu, M. Barnell, G.-L. Li, H. L. Xin, R. S. Williams, Q. Xia, J. J. Yang, *Nat. Mater.* **2016**, *16*, 101.
[45] S. Menzel, P. Kaupmann, R. Waser, *Nanoscale* **2015**, *7*, 12673.
[46] I. Valov, G. Staikov, *J. Solid State Electrochem.* **2013**, *17*, 365.
[47] T. Tsuruoka, K. Terabe, T. Hasegawa, M. Aono, *Nanotechnology* **2010**, *21*, 425205.

[48] S. Menzel, B. Klopstra, C. Kügeler, U. Böttger, G. Staikov, R. Waser, *MRS Online Proc. Library* **2009**, *1160*, 101.
[49] M. Luebben, S. Menzel, S. G. Park, M. Yang, R. Waser, I. Valov, *Nanotechnology* **2017**, *28*, 135205.
[50] E. Covi, W. Wang, Y.-H. Lin, M. Farronato, E. Ambrosi, D. Ielmini, *IEEE Trans. Electron Devices* **2021**, *68*, 4335.
[51] W. Wang, E. Covi, Y. H. Lin, E. Ambrosi, A. Milozzi, C. Sbandati, M. Farronato, D. Ielmini, *IEEE Trans. Electron Devices* **2021**, *68*, 4342.
[52] T. Liu, M. Verma, Y. Kang, M. Orlowski, *Appl. Phys. Lett.* **2012**, *101*, 073510.
[53] J. Yoo, J. Song, H. Hwang, *Nanotechnology* **2018**, *29*, 365707.
[54] Y. Li, J. Tang, B. Gao, W. Sun, Q. Hua, W. Zhang, X. Li, W. Zhang, H. Qian, H. Wu, *Adv. Sci.* **2020**, *7*, 2002251.
[55] Z. Wang, M. Rao, R. Midya, S. Joshi, H. Jiang, P. Lin, W. Song, S. Asapu, Y. Zhuo, C. Li, H. Wu, Q. Xia, J. J. Yang, *Adv. Funct. Mater.* **2018**, *28*, 1704862.
[56] X. Zhang, W. Wang, Q. Liu, X. Zhao, J. Wei, R. Cao, Z. Yao, X. Zhu, F. Zhang, H. Lv, S. Long, M. Liu, *IEEE Electron Device Lett.* **2018**, *39*, 308.
[57] D. Lee, M. Kwak, K. Moon, W. Choi, J. Park, J. Yoo, J. Song, S. Lim, C. Sung, W. Banerjee, H. Hwang, *Adv. Electron. Mater.* **2019**, *5*, 1800866.
[58] W. Wang, E. Covi, A. Milozzi, M. Farronato, S. Ricci, C. Sbandati, G. Pedretti, D. Ielmini, *Adv. Intell. Syst.* **2021**, *3*, 2000224.
[59] S. Menzel, S. Tappertzhofen, R. Waser, I. Valov, *Phys. Chem. Chem. Phys.* **2013**, *15*, 6945.
[60] J. van den Hurk, S. Menzel, R. Waser, I. Valov, *J. Phys. Chem. C* **2015**, *119*, 18678.
[61] Juelich Aachen Resistive Switching Tools [JART]. Techreport Juelich Aachen Research Alliance. http://www.emrl.de/JART.html#:~:text=Our%20laboratories%20provide%20simulation%20models,circuit%20designers%20or%20device%20engineers (accessed: November 2021).
[62] Y. Sun, X. Zhao, C. Song, K. Xu, Y. Xi, J. Yin, Z. Wang, X. Zhou, X. Chen, G. Shi, H. Lv, Q. Liu, F. Zeng, X. Zhong, H. Wu, M. Liu, F. Pan, *Adv. Funct. Mater.* **2019**, *29*, 1808376.
[63] M. Lübben, I. Valov, *Adv. Electron. Mater.* **2019**, *5*, 1800933.
[64] C. Schindler, I. Valov, R. Waser, *Phys. Chem. Chem. Phys.* **2009**, *11*, 5974.
[65] J. Yoo, J. Park, J. Song, S. Lim, H. Hwang, *Appl. Phys. Lett.* **2017**, *111*, 063109.
[66] Y. Yang, P. Gao, S. Gaba, T. Chang, X. Pan, W. Lu, *Nat. Commun.* **2012**, *3*, 732.
[67] S. Menzel, U. Böttger, R. Waser, *J. Appl. Phys.* **2012**, *111*, 014501.
[68] Y. Wang, Z. Zhang, H. Li, L. Shi, *J. Electron. Mater.* **2019**, *48*, 517.
[69] Y. Zhao, C. Fang, X. Zhang, X. Xu, T. Gong, Q. Luo, C. Chen, Q. Liu, H. Lv, Q. Li, F. Zhang, L. Li, M. Liu, *IEEE Trans. Electron Devices* **2018**, *65*, 4290.
[70] J. Yin, F. Zeng, Q. Wan, Y. Sun, Y. Hu, J. Liu, G. Li, F. Pan, *J. Phys. Chem. C* **2019**, *123*, 878.
[71] R. D. Nikam, K. G. Rajput, H. Hwang, *Small* **2021**, *17*, 2006760.
[72] X. Zhao, J. Ma, X. Xiao, Q. Liu, L. Shao, D. Chen, S. Liu, J. Niu, X. Zhang, Y. Wang, R. Cao, W. Wang, Z. Di, H. Lv, S. Long, M. Liu, *Adv. Mater.* **2018**, *30*, 1705193.
[73] F. Yuan, Z. Zhang, C. Liu, F. Zhou, H. M. Yau, W. Lu, X. Qiu, H.-S. P. Wong, J. Dai, Y. Chai, *ACS Nano* **2017**, *11*, 4097.
[74] H. Sun, Q. Liu, C. Li, S. Long, H. Lv, C. Bi, Z. Huo, L. Li, M. Liu, *Adv. Funct. Mater.* **2014**, *24*, 5679.
[75] Q. Hua, H. Wu, B. Gao, M. Zhao, Y. Li, X. Li, X. Hou, M.-F. Chang, P. Zhou, H. Qian, *Adv. Sci.* **2019**, *6*, 1900024.
[76] N. Shukla, B. Grisafe, R. K. Ghosh, N. Jao, A. Aziz, J. Frougier, M. Jerry, S. Sonde, S. Rouvimov, T. Orlova, S. Gupta, S. Datta, in *2016 IEEE Int. Electron Devices Meeting (IEDM)*, IEEE, Piscataway, NJ **2016**.
[77] Y.-F. Lu, Y. Li, H. Li, T.-Q. Wan, X. Huang, Y.-H. He, X. Miao, *IEEE Electron Device Lett.* **2020**, *41*, 1245.
[78] K. Wang, Q. Hu, B. Gao, Q. Lin, F. W. Zhuge, D. Y. Zhang, L. Wang, Y. H. He, R. H. Scheicher, H. Tong, X. S. Miao, *Mater. Horiz.* **2021**, *8*, 619.
[79] T. Fu, X. Liu, H. Gao, J. E. Ward, X. Liu, B. Yin, Z. Wang, Y. Zhuo, D. J. F. Walker, J. J. Yang, J. Chen, D. R. Lovley, J. Yao, *Nat. Commun.* **2020**, *11*, 1861/1.
[80] A. S. Sokolov, M. Ali, R. Riaz, Y. Abbas, M. J. Ko, C. Choi, *Adv. Funct. Mater.* **2019**, *29*, 1807504.
[81] G. Dastgeer, H. Abbas, D. Y. Kim, J. Eom, C. Choi, *Phys. Status Solidi RRL* **2021**, *15*, 2000473.
[82] H. Abbas, Y. Abbas, G. Hassan, A. S. Sokolov, Y. R. Jeon, B. Ku, C. J. Kang, C. Choi, *Nanoscale* **2020**, *12*, 14120.
[83] A. Hardtdegen, H. Zhang, S. Hoffmann-Eifert, *ECS Trans.* **2016**, *75*, 177.
[84] A. C. Dippel, O. Gutowski, L. Klemeyer, U. Boettger, F. Berg, T. Schneller, A. Hardtdegen, S. Aussen, S. Hoffmann-Eifert, M. V. Zimmermann, *Nanoscale* **2020**, *12*, 13103.